Normal, dust-obscured galaxies in the epoch of reionization

Fudamoto, Y.; Oesch, P. A.; Schouws, S.; Stefanon, M.; Smit, R.; Bouwens, R. J.; Bowler, R. A. A.; Endsley, R.; Gonzalez, V.; Inami, H.

Link to publication in University of Groningen/UMCG research database

Article

Normal, dust-obscured galaxies in the epoch of reionization

Check for updates

Y. Fudamoto[1,2,3 ✉], P. A. Oesch[1,4], S. Schouws[5], M. Stefanon[5], R. Smit[6], R. J. Bouwens[5], R. A. A. Bowler[7], R. Endsley[8], V. Gonzalez[9,10], H. Inami[11], I. Labbe[12], D. Stark[8], M. Aravena[13], L. Barrufet[1], E. da Cunha[14,15], P. Dayal[16], A. Ferrara[17], L. Graziani[18,20,27], J. Hodge[5], A. Hutter[16], Y. Li[21,22], I. De Looze[23,24], T. Nanayakkara[12], A. Pallottini[17], D. Riechers[25], R. Schneider[18,19,26,27], G. Ucci[16], P. van der Werf[5] & C. White[8]

Over the past decades, rest-frame ultraviolet (UV) observations have provided large samples of UV luminous galaxies at redshift (z) greater than 6 (refs. [1–3]), during the so-called epoch of reionization. While a few of these UV-identified galaxies revealed substantial dust reservoirs[4–7], very heavily dust-obscured sources at these early times have remained elusive. They are limited to a rare population of extreme starburst galaxies[8–12] and companions of rare quasars[13,14]. These studies conclude that the contribution of dust-obscured galaxies to the cosmic star formation rate density at $z > 6$ is sub-dominant. Recent ALMA and Spitzer observations have identified a more abundant, less extreme population of obscured galaxies at $z = 3–6$ (refs. [15,16]). However, this population has not been confirmed in the reionization epoch so far. Here, we report the discovery of two dust-obscured star-forming galaxies at $z = 6.6813 \pm 0.0005$ and $z = 7.3521 \pm 0.0005$. These objects are not detected in existing rest-frame UV data and were discovered only through their far-infrared [C II] lines and dust continuum emission as companions to typical UV-luminous galaxies at the same redshift. The two galaxies exhibit lower infrared luminosities and star-formation rates than extreme starbursts, in line with typical star-forming galaxies at $z \approx 7$. This population of heavily dust-obscured galaxies appears to contribute 10–25% to the $z > 6$ cosmic star formation rate density.

As part of the ongoing ALMA large program REBELS (Reionization-Era Bright Emission Line Survey), we are observing 40 UV-luminous primary targets at $z > 6.5$ (ref. [17]). Among these targets are REBELS-12 and REBELS-29. When inspecting the ALMA data cube of these two sources, we identified two additional emission line neighbours.

The primary targets of our ALMA observing program, REBELS-12 and REBELS-29, represent some of the most UV-luminous galaxies in this redshift range, and have $M_{UV} = -22.5 \pm 0.3$ and -22.2 ± 0.1. They were originally identified with a photometric redshift of $z_{phot} = 6.82^{+0.13}_{-0.11}$ and $z_{phot} = 7.40^{+0.15}_{-0.21}$, respectively, based on deep ground based optical and near-infrared (NIR) data. The ALMA observations were carried out on 24 and 29 November 2019, targeting the singly ionized carbon emission line, [C II] 158 μm and dust continuum emission with a frequency coverage of the vast majority of the photometric redshift probability distribution. The ALMA observations reached emission line sensitivities of 0.19 mJy beam^{-1} and 0.16 mJy beam^{-1} per 100 km s^{-1} spectral element for REBELS-29 and REBELS-12, respectively. This resulted in clear [C II] emission line detections of both sources, at frequencies perfectly consistent with the photometric redshift estimations (see Fig. 1 and Extended Data Fig. 1). The integrated flux densities of these lines are 0.44 Jy kms^{-1} and 1.20 Jy kms^{-1} corresponding to point source detection significances of 9.2σ and 6.3σ, respectively. These lines yield a spectroscopic redshift of $z = 6.6847 \pm 0.0002$ and $z = 7.347 \pm 0.001$ for REBELS-29 and REBELS-12, respectively.

The [C II] line integrated maps of these galaxies revealed two strong, serendipitous emission lines at ~7.4 and ~11.5 arcsec offset from the primary targets, corresponding to 40 pkpc (proper kiloparsecs) and 58 pkpc, respectively. The continuum subtracted spectra then
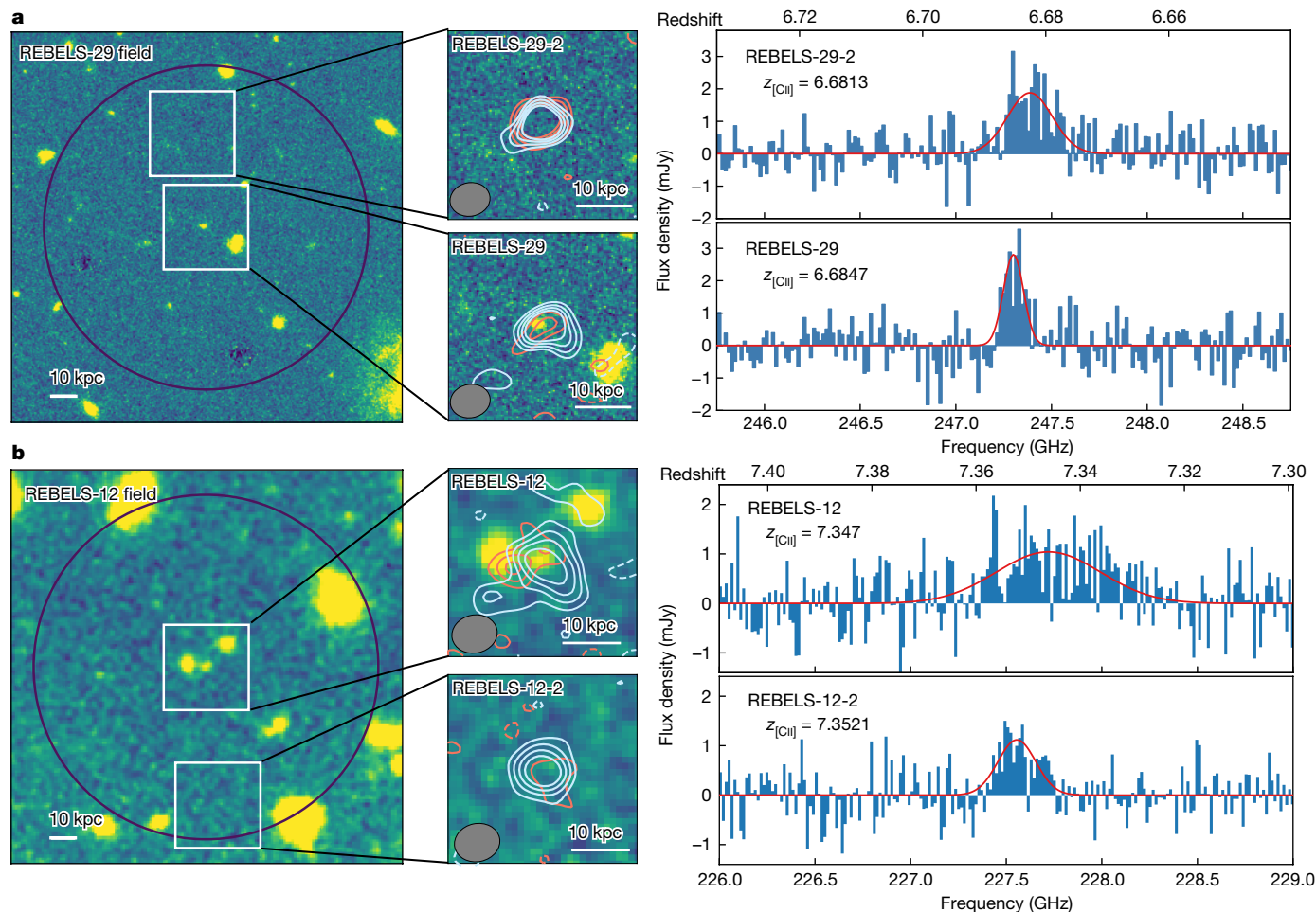
Fig. 1 | [C II] 158 μm line and dust emission detections. a, REBELS-29 field at z ≈ 6.68. **b**, REBELS-12 field at z ≈ 7.35. Background images are HST F140W and VIDEO J-band, respectively. Black circles show the half power beam widths of each ALMA pointing (~13 arcsec radius), and white squares indicate 6.5-arcsec-wide boxes that are shown in the middle panels. White horizontal bars correspond to 10 pkpc. Solid red and light blue contours show 2σ to 5σ levels (and −5σ to −2σ for dashed contours) for the continuum and [C II] moment-0 maps, respectively. The continuum subtracted [C II] spectra are shown at the native velocity resolution of 20 km s⁻¹. The two sources REBELS-29-2 and REBELS-12-2 were found serendipitously as companions to the central, UV-luminous targets, with emission lines at almost exactly the same frequencies as the central targets, accompanied with dust continuum emission at the same location. Their spatial and spectral proximity, and absence in optical/NIR images confirms these companions as unexpected, dusty star-forming sources in the epoch of reionization.

confirmed that the additional emission lines emerge at almost exactly the same frequency as the central targets (velocity offsets of 110 km s⁻¹ and 210 km s⁻¹ for REBELS-29 and REBELS-12, respectively; see right panels of Fig. 1). Hereafter, we call these additional line sources REBELS-12-2 and REBELS-29-2.

After correcting for the primary beam attenuation, these emission lines have integrated flux densities of 0.781 Jy kms⁻¹ and 0.581 Jy kms⁻¹, corresponding to a detection significance of 9.7σ and 6.8σ in the

moment-0 maps for REBELS-29-2 and REBELS-12-2, respectively. Additionally, REBELS-29-2 has a clear (9.2σ) dust continuum detection, while only a tentative (2.8σ) continuum signal is found for REBELS-12-2. These measurements correspond to flux densities of 192 ± 25 μJy and 110 ± 52 μJy after applying primary beam and cosmic microwave background (CMB) corrections, respectively (see Extended Data Table 1).

Given the significance of the emission line detections and the number of independent beams in the moment-0 maps, the probability of a random

Table 1 | Summary of galaxy properties.

Galaxy name	Redshift[b]	RA (deg)	Dec (deg)	Stellar mass ($10^9 M_\odot$)	SFR$_{UV}$ ($M_\odot$ yr⁻¹)	SFR$_{IR}$[c] ($M_\odot$ yr⁻¹)	SFR$_{[CII]}$ ($M_\odot$ yr⁻¹)
REBELS-29[a]	6.6847 ± 0.0002	150.403542	2.630306	10^{+3}_{-3}	35 ± 3	$22.4^{+18.8}_{-10.5}$	61.0 ± 7.0
REBELS-29-2	6.6813 ± 0.0005	150.403875	2.632339	< 25	< 2	$74.3^{+47.0}_{-31.2}$	100.0 ± 11.2
REBELS-12	7.347 ± 0.001	36.2830833	−5.111316	19^{+9}_{-7}	41±3	$70.5^{+51.6}_{-31.3}$	163.0 ± 31.5
REBELS-12-2	7.3521 ± 0.0005	36.2828333	−5.114225	< 10	< 14.7	$43.1^{+37.0}_{-22.7}$	88.0 ± 16.6

[a]ID304384 in Bowler et al. (2018)[18].
[b]Spectroscopic redshift measured from [C II] 158 μm emission lines.
[c]Based on L_{IR} estimates with conservative error bars (see Supplementary Information).
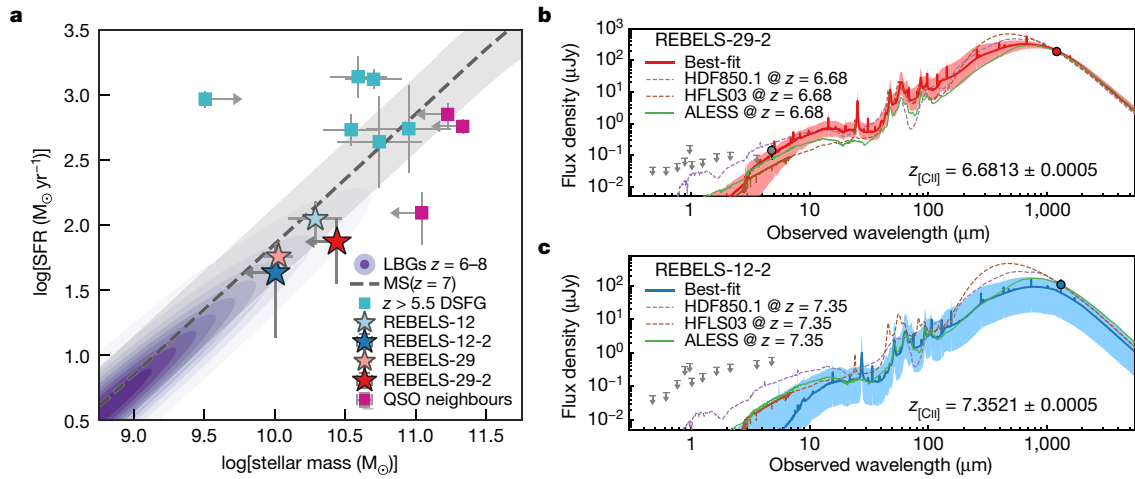
Fig. 2 | Estimated properties of REBELS-29-2 and REBELS-12-2.
a, Star-formation rate as a function of stellar mass for $z > 5.5$ galaxies. Background contours show the distribution of faint LBGs at $z = 6$–8. The dashed line and shaded region indicates the star-forming main-sequence as measured up to $z \approx 4$ and extrapolated to $z = 7$ (ref. [19]). Cyan squares represent previously identified dusty star-forming galaxies (DSFGs) at $z \approx 5.7$–6.9. Purple squares show dusty galaxies found as companions of $z \approx 6.1$–6.5 quasars, which also remained undetected in rest-UV observations. Their mass limits are estimated from dynamical masses[13,14]. Error bars correspond to 1σ uncertainties. The UV-bright galaxies (REBELS-12 and REBELS-29), and the serendipitous, dusty galaxies (REBELS-12-2 and REBELS-29-2) are shown as blue and red stars (using

SFR$_{IR}$). The SFRs and stellar mass limits of the newly identified galaxies are lower than the majority of $z > 5.5$ DSFGs and quasar companions at these redshifts. **b**, **c**, Photometric constraints and SEDs of REBELS-29-2 and REBELS-12-2, respectively. 2σ upper limits are shown for non-detections (grey arrows). Red and blue solid lines show the median posterior SEDs together with their 68% confidence contours. For comparison, SEDs of dusty star-bursting galaxies normalized at the ALMA continuum fluxes are indicated in solid green (the average SED of ALESS galaxies[20]), dashed brown (HFLS03[8]), and dashed purple lines (HDF850.1)[21]. The newly found dusty sources as companions of normal star-forming galaxies suggest that dusty, lower-luminosity versions of DSFGs exist at $z = 6$–8 in larger number than previously assumed.
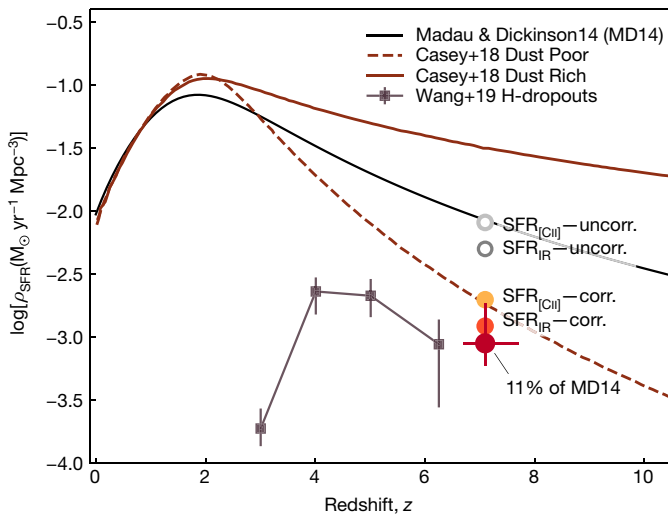

Fig. 3 | Contribution of obscured galaxies to the cosmic SFR density ρ_{SFR}.
The black solid line shows the consensus estimate ρ_{SFR}^{MD14} as a function of redshift[1], which at $z > 4$ is derived from LBGs with a small dust correction. The dark-red solid and dashed lines indicate two possible models for the extra contribution from obscured sources[22], which can be constrained from our observations. Error bars correspond to 1σ uncertainties. At most, the dusty $z \approx 7$ galaxies identified here could contribute 60–100% of ρ_{SFR}^{MD14} depending on the exact estimate of their SFRs (dark-grey, SFR$_{IR}$; light-grey, SFR$_{[CII]}$). However, when correcting these values for the expected excess due to clustering, they lie around four times lower (light-red and orange dots). A similar SFRD estimate is found from the fraction of [C II]-confirmed REBELS targets that show a dusty companion (11%; dark-red). All these estimates are consistent with Spitzer-selected, massive dusty galaxies at $z \approx 3$–6 (squares[15]). While the exact SFRD contributed by dust-obscured sources is still uncertain, their existence in the epoch of reionization implies a revision of our understanding of early galaxy assembly.

Gaussian noise fluctuation is negligible. Furthermore, the co-spatial continuum signals confirm that these blind line detections are real. In the Methods, we estimate the probability of finding an unassociated, random emission line almost exactly at the same frequency as a primary one in an ALMA data cube to be extremely small ($p < 6 \times 10^{-4}$). Therefore, this strongly suggests that these serendipitous detections stem from neighbouring sources sitting in the same environment as the primary targets. The [C II] 158 μm redshifts of REBELS-29-2 and REBELS-12-2 are thus $z = 6.6813 \pm 0.0002$ and $z = 7.3521 \pm 0.0005$, respectively.

REBELS-29-2 and REBELS-12-2 are covered by deep optical/NIR observations, corresponding to rest-frame UV/optical wavelengths. However, neither source shows any optical counterpart (Fig. 1 and Extended Data Fig. 2) except for a tentative (~2σ) Spitzer IRAC 4.5 μm detection of REBELS-29-2. These non-detections in rest-frame UV/optical bands indicate that these serendipitously found [C II] line emitters are heavily dust-obscured galaxies.

Star-formation rates (SFRs) are estimated based on the UV and far-infrared (FIR) luminosities. However, due to the non-detections in rest-UV data we can only provide limits on the UV-based SFRs, for which we find SFR$_{UV}$ < 2 $M_\odot$ yr^{-1} and SFR$_{UV}$ < 14.7 $M_\odot$ yr^{-1} (at 2σ), where $M_\odot$ is the mass of the sun; the IR-based SFRs from the ALMA dust continuum amount to SFR$_{IR}$ = 74.3$^{+47.0}_{-31.2}$ and 43.1$^{+37.0}_{-22.7}$ $M_\odot$ yr^{-1} for REBELS-29-2 and REBELS-12-2, respectively. We hereafter use the SFRs directly derived from FIR luminosities as our fiducial SFRs (for more information, see Methods).

Given the optical non-detections of REBELS-29-2 and REBELS-12-2, also their stellar masses cannot be accurately constrained. We only derive upper limits from spectral energy distribution (SED) fitting (see Methods). The estimated SFRs and stellar mass limits are consistent with normal ~$L*$ Lyman break galaxies (LBGs) at $z > 6$ selected from rest-frame UV data such as the REBELS primary target sample, which define the so-called main-sequence of star-formation[19] (Fig. 2).

The serendipitous discovery of these two dusty galaxies at $z \approx 7$ shows that our current (UV-based) census of very early galaxies is

still incomplete. It is thus crucial to estimate the contribution of such sources to the total cosmic SFR density (SFRD). However, this is not a trivial task given that these sources were only found as neighbours to UV-luminous primary targets. We therefore provide several different estimates (see Methods for details). Assuming that REBELS-29-2 and REBELS-12-2 were found in a completely blind survey consisting of all REBELS data-cubes and using their UV+IR-based SFRs, their SFRD would amount to ~60–100% of the total SFRD contributed from UV-selected LBGs, ρ_{LBG} (ref.[1]) (Fig. 3). However, given that these sources were in fact detected as clustered galaxies in a targeted follow-up survey, we have to account for the excess probability of finding such sources based on the correlation function. Doing this, we estimate that the actual contribution by these sources to the SFRD is reduced by a factor 4.1 ± 0.6, that is, amounting to ~10–25% of ρ_{LBG}.

An independent, conservative estimate of their SFRD contribution can be obtained from the fraction of primary UV-luminous targets with confirmed [C II] lines that revealed such a dusty neighbour (2 out of 19, that is, $10.5^{+9.1}_{-5.0}$%). Assuming that this fraction also applies to fainter sources, this would result in an additional SFRD of $8.9^{+7.7}_{-4.3} \times 10^{-4}\ M_{\odot}\,yr^{-1}\,Mpc^{-3}$, that is, ~11% of UV-luminous sources. All these estimates are starting to constrain different models for the contribution of dust-obscured sources at high redshifts[22] (see Fig. 3). It is clear, however, that a blind, wide-area survey for such sources is required in the future to properly constrain their number density in blank fields. These surveys must observe substantially deeper than had been envisioned previously[23] to sample the fainter dust-obscured, but otherwise 'normal' galaxies such as REBELS-12-2 and REBELS-29-2.

Online content

Any methods, additional references, Nature Research reporting summaries, source data, extended data, supplementary information, acknowledgements, peer review information; details of author contributions and competing interests; and statements of data and code availability are available at https://doi.org/10.1038/s41586-021-03846-z.

1. Madau, P. & Dickinson, M. Cosmic star-formation history. *Annu. Rev. Astron. Astrophys.* **52**, 415–486 (2014).
2. Bouwens, R. J. et al. UV luminosity functions at redshifts z ~ 4 to z ~ 10: 10,000 galaxies from HST legacy fields. *Astrophys. J.* **803**, 34 (2015).
3. Ono, Y. et al. Great optically luminous dropout research using subaru HSC (GOLDRUSH). I. UV luminosity functions at z ~ 4–7 derived with the half-million dropouts on the 100 deg² sky. *Publ. Astron. Soc. Jpn.* **70**, S10 (2018).
4. Watson, D. et al. A dusty, normal galaxy in the epoch of reionization. *Nature* **519**, 327–330 (2015).
5. Hashimoto, T. et al. Big three dragons: a z = 7.15 Lyman-break galaxy detected in [O III] 88 μm, [C II] 158 μm, and dust continuum with ALMA. *Publ. Astron. Soc. Jpn.* **71**, 71 (2019).
6. Tamura, Y. et al. Detection of the far-infrared [O III] and dust emission in a galaxy at redshift 8.312: early metal enrichment in the heart of the reionization era. *Astrophys. J.* **874**, 27 (2019).
7. Bakx, T. J. L. C. et al. ALMA uncovers the [C II] emission and warm dust continuum in a z = 8.31 Lyman break galaxy. *Mon. Not. R. Astron. Soc.* **493**, 4294–4307 (2020).
8. Riechers, D. A. et al. A dust-obscured massive maximum-starburst galaxy at a redshift of 6.34. *Nature* **496**, 329–333 (2013).
9. Strandet, M. L. et al. ISM properties of a massive dusty star-forming galaxy discovered at z ~ 7. *Astrophys. J. Lett.* **842**, L15 (2017).
10. Marrone, D. P. et al. Galaxy growth in a massive halo in the first billion years of cosmic history. *Nature* **553**, 51–54 (2018).
11. Dudzevičiūtė, U. et al. An ALMA survey of the SCUBA-2 CLS UDS field: physical properties of 707 sub-millimetre galaxies. *Mon. Not. R. Astron. Soc.* **494**, 3828–3860 (2020).
12. Riechers, D. A. et al. COLDz: a high space density of massive dusty starburst galaxies ~ 1 billion years after the big bang. *Astrophys. J.* **895**, 81 (2020).
13. Decarli, R. et al. Rapidly star-forming galaxies adjacent to quasars at redshifts exceeding 6. *Nature* **545**, 457–461 (2017).
14. Mazzucchelli, C. et al. Spectral energy distributions of companion galaxies to z ~ 6 quasars. *Astrophys. J.* **881**, 163 (2019).
15. Wang, T. et al. A dominant population of optically invisible massive galaxies in the early Universe. *Nature* **572**, 211–214 (2019).
16. Williams, C. C. et al. Discovery of a dark, massive, ALMA-only galaxy at z ~ 5–6 in a tiny 3 mm survey. *Astrophys. J.* **884**, 154 (2019).
17. Bouwens, R. J. et al. Reionization era bright emission line survey: selection and characterization of luminous interstellar medium reservoirs in the z>6.5 Universe. Preprint at https://arxiv.org/abs/2106.13719 (2021).
18. Bowler, R. A. A. et al. Obscured star formation in bright z = 7 Lyman-break galaxies. *Mon. Not. R. Astron. Soc.* **481**, 1631–1644 (2018).
19. Schreiber, C. et al. The Herschel view of the dominant mode of galaxy growth from z = 4 to the present day. *Astron. Astrophys.* **575**, A74 (2015).
20. Swinbank, A. M. et al. An ALMA survey of sub-millimetre galaxies in the Extended Chandra Deep Field South: the far-infrared properties of SMGs. *Mon. Not. R. Astron. Soc.* **438**, 1267–1287 (2014).
21. Walter, F. et al. The intense starburst HDF 850.1 in a galaxy overdensity at z ≈ 5.2 in the Hubble Deep Field. *Nature* **486**, 233–236 (2012).
22. Casey, C. M. et al. The brightest galaxies in the dark ages: galaxies' dust continuum emission during the reionization era. *Astrophys. J.* **862**, 77 (2018).
23. Zavala, J. A. et al. The evolution of the IR luminosity function and dust-obscured star formation over the past 13 billion years. *Astrophys. J.* **909**, 165 (2021).

Methods

Cosmology
Throughout this paper we assume a concordance cosmology with $\Omega_m = 0.3$, $\Omega_\Lambda = 0.7$, $h = 0.7$.

Target selection
REBELS-12 and REBELS-29 are among the sample selected in the ALMA large program REBELS (Reionization-Era Bright Emission Line Survey). The entire sample of the REBELS program consists of 40 UV-luminous galaxies ($\gtrsim 2 \times L_*$) with photometric redshifts at $z \approx 6.5$–9. The corresponding UV-derived SFRs are in excess of ~30 $M_\odot$ yr^{-1}, but they still correspond to 'normal' star-forming galaxies, that is, they lie on the main-sequence of star-formation. An additional, important criterion for choosing the targets was a small uncertainty on their photometric redshifts to maximize the efficiency of the overall survey. The REBELS program is still ongoing, with ~85% of the final data acquired so far. For this paper, we exploit the current dataset taken during cycle 7.

Observations and reduction of ALMA data
Our ALMA observations were performed as part of the project 2019.1.01634.L during ALMA cycle 7. To scan the whole redshift probability of [C II] 158 μm emission lines, the receivers were tuned to cover 243.13 – 250.63 GHz for REBELS-29, and 217.91 – 238.29 GHz for REBELS-12. In each frequency setup, the correlator was set to frequency domain mode with a band width of 1,875 MHz in each spectral window, to sufficiently resolve [C II] emission lines. The observations were carried out in ALMA configuration C43-2, with projected baselines ranging from 14 m to 313 m. With our observing frequency, flux calibration errors are <10%.

The data were calibrated using the standard ALMA calibration pipeline implemented in the Common Astronomy Software Applications package (CASA) version 5.6.1. We imaged the continuum and data cubes using the CASA task tclean with natural weighting to maximize point source sensitivity. The resulting synthesized beam sizes were 1.15″ × 1.38″ and 1.25″ × 1.51″ for REBELS-29 and REBELS-12, respectively. During the imaging process, the synthesized beam is deconvolved by applying a source detection threshold of three times the background root mean square of dirty images. Because there are no extremely bright sources in our cubes and the side lobes of the synthesized beam contribute <10% of the sensitivity, the exact choice of the cleaning threshold does not affect our image products.

After subtracting the continuum using the CASA task uvcontsub, we extracted spectra in an iterative way to create robust apertures for the extraction. From the extracted spectra, we created the moment-0 map spanning over ± 2σ velocity width of the emission line. In the next iteration, any other pixels with positive signals down to 2σ were added and the spectra were re-extracted. This iteration continued until the integrated emission line flux converged. In all cases a few iterations were enough to achieve this.

Optical and NIR data
Optical and NIR images are obtained from publicly available surveys. In particular, REBELS-29 lies in the 2 deg^2 COSMOS field covered by Ultra-VISTA[24], and REBELS-12 is in the VIDEO survey[25] within the XMM-Newton Large-Scale Structure (XMM-LSS) field 3. Both of these fields thus have relatively deep, ground-based NIR imaging data in the YJHK$_s$ bands, from which the primary REBELS sources are selected. We use the DR4 images of the UltraVISTA survey. The 5σ limiting magnitudes in the J band are thus 26.0 and 24.9, respectively. REBELS-29 is covered by deep optical images with Megacam from the Canada–France–Hawaii Legacy Survey (CFHTLS[26]) and both sources have additional optical imaging from the Subaru Hyper Suprime-Cam (HSC) survey[27]. These fields have also been observed with Spitzer/IRAC from various programs over

the past few years. In the VIDEO field only 3.6 μm and 4.5 μm data are available, while COSMOS has also been covered with IRAC at 5.8 μm and 8.0 μm. In 3.6 μm, the 5σ limiting magnitudes measured in 2″.8 diameter apertures are 25.5 and 24.3 mag, respectively. For more details on the ground-based and Spitzer imaging over these fields see Bowler et al.[28] and Stefanon et al.[29] Additionally, REBELS-29 is covered by HST observations in the F140W filter[30], reaching a 5σ depth of 26.9 mag. We combine all the available data to constrain the panchromatic SEDs of both the primary REBELS targets as well as the serendipitous, dusty companions.

Derivation of physical parameters
Star formation rates. SFRs are estimated based on the UV and FIR luminosities (including conservative assumptions about the IR SED shapes; see the section below and Extended Data Table 1). Alternatively, we also estimate SFRs based on the correlation between SFR and $L_{\text{[CII]}}$, previously measured at $4 < z < 6$ (ref. [31]) and $z \approx 0$ (ref. [32]). While this [C II] approach yields slightly higher values of $100 \pm 11\,M_\odot$ yr^{-1} and $88 \pm 17\,M_\odot$ yr^{-1}, respectively, they are still consistent within uncertainties with those derived from the UV and IR continuum (Table 1). Given the uncertain calibration of the $L_{\text{[CII]}}$–SFR correlation of high-redshift galaxies, we use the SFRs directly derived from FIR luminosities as our fiducial SFRs.

Stellar mass limits. To interpret the serendipitous dusty galaxies, we estimate upper limits for their stellar masses based on their optical, NIR and FIR photometry and SED modelling. These limits are further tested with dynamical mass estimations.

We use the publicly available code Bayesian Analysis of Galaxies for Physical Inference and Parameter EStimation (BAGPIPES[33]) to derive SEDs consistent with all linear flux measurements and their uncertainties (see Extended Data Table 2), while the redshifts are fixed to the [C II] detections. The input stellar population synthesis models for BAGPIPES are based on the 2016 version of the Bruzual and Charlot library[34], using a Kroupa[35] initial mass function. We adopt constant star formation history models with formation time as a free parameter, and we allow for metallicities ranging from 0.1 to 2.5 × $Z_\odot$, where $Z_\odot$ represents the solar metallicity. Nebular continuum and line emission are added in a self-consistent manner[36] based on the photoionization code CLOUDY[37] using the ionization parameter (log$U$) as a free parameter. Dust attenuation is included using the standard attenuation law for star-forming galaxies[38], with the attenuation in the V-band (A_V) as a free parameter. We have also tested the impact of using a different dust attenuation model[39], but obtained consistent mass limits. Differential dust attenuation is allowed for stars in their birth clouds by a multiplicative factor (η). Dust emission is then included self-consistently using a grid of SED models[40] under the assumption of energy balance, that is, that the dust-absorbed energy is re-radiated in the FIR. The dust emission model has three parameters: the minimum intensity of starlight incident on the dust ($U_{\min}$), the fraction of dust particles at this lowest intensity (γ), and the amount of PAH emission (q_{PAH}). Overall, these SED fits thus have nine free parameters, for which we assumed very wide, uniform priors (see Extended Data Table 3 for input priors). With the current optical/NIR data we do not expect to constrain all these free parameters for the dust-obscured sources. However, our approach allows us to marginalize over these parameters in order to derive realistic upper limits of stellar masses. Through this analysis, we find 90% probability upper limits of log$M_*/M_\odot < 10.4(10.0)$ for REBELS-29-2 (REBELS-12-2). The results are listed in Table 1 in the main text and the posterior SEDs are shown in Fig. 2 and Extended Data Fig. 1.

Additionally, we derive dynamical masses to test the above stellar mass limits from SED analyses. While dynamical masses are very uncertain given the current low-resolution observations, they can provide a useful, independent check. In particular, we estimated dynamical

Article

masses using the [C II] 158 μm emission velocity dispersion (Table 1) and [C II] emission sizes. [C II] emission sizes are measured using CASA task uvmodelfit assuming a two-dimensional Gaussian with free parameters of total fluxes and full width at half maximum (FWHM) while centroids are fixed. REBELS-29-2 is unresolved and thus consistent with a point source in our resolution. To estimate the upper limit of dynamical masses of REBELS-29-2, we therefore assumed a synthesized beam FWHM as an upper limit size of REBELS-29-2. REBELS-12-2 is marginally resolved with the best fit Gaussian FWHM of $1.7''(\pm 0.8'') \times 1.0''(\pm 1.0'')$ with a position angle of 6.3 ± 40 degree. Following previous studies[41,42], we used a simplified dynamical mass estimate, namely: $M_{\rm dyn} = 1.165 \times 10^5 \, v_{\rm circ}^2 \, D$ where D is a [C II] emission diameter in kpc, and the circular velocity $v_{\rm circ}$ is approximated using velocity dispersion ($\sigma_{\rm [CII]}$) and inclination angle i as $v_{\rm circ} = 1.763 \times \sigma_{\rm [CII]}/\sin(i)$. For the inclination angles, as the low-resolution observations only provide unconstrained or uncertain values, we assumed a uniform distribution of $\sin(i) = 0.45 - 1$ as an approximation from a dispersion dominated system to an edge-on disk[42]. In this way, we found dynamical masses of $<1.1 \times 10^{11} M_\odot$, and $9.4^{+10.9}_{-5.3} \times 10^{10} \, M_\odot$. Assuming gas mass fraction of 60%[43], these dynamical masses provide stellar mass constraints of $<6.6 \times 10^{10} \, M_\odot$, and $3.4^{+6.6}_{-3.1} \times 10^{10} \, M_\odot$ for REBELS-29-2 and REBELS-12-2, respectively. While still uncertain, these estimates are thus higher, but completely consistent with the stellar mass upper limits from the panchromatic SED analyses.

Infrared luminosity and dust masses

Using the rest-frame -158 μm continuum measurements we estimated total infrared ($\lambda = 8$–$1,000$ μm) luminosities following previous works[42,44], which assume a range of grey body models consistent with galaxies observed at $z < 6$ (refs. [45,46]). In particular, we use SEDs for which the optical depth reaches unity at $\lambda_0 = 100$ μm. To construct FIR SED models, we assumed the following parameters: α the blue power-law, β the long wavelength slope, and $T_{\rm SED}$ the luminosity weighted dust temperature. We assumed a very conservative range of these parameters uniformly distributed between $\alpha = 1.5 - 2.5$, $\beta = 1.5 - 2.5$, and $T_{\rm SED} = 35 - 73$ K. The range of luminosity weighted dust temperatures $T_{\rm SED}$ used here corresponds to a range of 'peak temperatures' of $T_{\rm peak} \simeq 30 - 50$ K, as calculated from the peak wavelength of the SED and assuming Wien's displacement law ($T_{\rm peak}$ [K] $= 2.9 \times 10^3/\lambda_{\rm peak}$ [μm]). Using the assumed parameter distributions, we normalized the FIR SEDs to the ALMA continuum fluxes at the observed wavelength of $\lambda_{\rm obs} = 1,248$ μm and $\lambda_{\rm obs} = 1,315$ μm for galaxies in the REBELS-29 and REBELS-12 fields, respectively, and calculated IR luminosity distributions. We derived IR luminosities from the obtained IR luminosity distributions by calculating the posterior median, 16th percentile and 84th percentile values. In both the IR luminosity and dust mass calculations (see next paragraph), we applied corrections due to the CMB heating and CMB against which we observe the dust continuum[47]. The results are listed in Extended Data Table 1.

We derived dust masses using the same distribution of SED parameters assuming a dust mass absorption coefficient of $\kappa_{\rm d}(\lambda_{\rm rest}) = 0.77 \times ((1+z) \times 850/\lambda_{\rm obs})^\beta$ cm^2 g^{-1} at the observed wavelength of $\lambda_{\rm obs} = 1,248$ μm and $\lambda_{\rm obs} = 1,315$ μm for galaxies in REBELS-29 and REBELS-12 fields, respectively. In particular, we assumed that the mass-weighted dust temperatures have the same conservative distribution as the luminosity weighted dust temperatures. The estimated dust masses are $M_{\rm dust} = 2.2^{+2.2}_{-1.1} \times 10^7$ and $1.2^{+1.7}_{-0.8} \times 10^7 \, M_\odot$, consistent with previous studies of sources at similar redshift[4,48]. Note that these masses are likely to be lower limits of the total dust budget, as diffuse and relatively cold dust components would be in thermal equilibrium with the CMB[49–51] and thus invisible from observations. Nevertheless, even with the current dust mass estimates, $>16 - 50$ % of metals ever produced by supernovae in these sources are already locked into dust grains, consistent with local Universe values[52]. This suggests very fast dust build-up at $z > 6$ (refs. [53,54]), which will be further investigated in a follow-up paper.

Possible lower redshift contamination?

In the main text, we argued that the two serendipitously detected sources lie at the same redshift as the primary REBELS targets. The main reason for this is that galaxies in the Universe are clustered and that the emission lines lie at almost exactly the same frequency (within less than 0.2 GHz) of the main targets' lines, corresponding to velocity offsets of <250 km s^{-1}. Here, we further quantify the probability of detecting a lower redshift source that has an emission line within 0.2 GHz of the primary target's [C II] frequency and within the half-primary beam width (HPBW) of our ALMA observations (-13 arcsec radius). We base this analysis on the ALMA continuum detections of the two sources, and the IR luminosity functions (LFs) measured at lower redshifts[55]. The most likely candidate for random emission lines are transitions of CO. However, we also test other lines that have been detected in distant galaxies[56]. For each possible line, we compute the corresponding source redshift and then convert the ALMA continuum emission to a total infrared luminosity using the same template SED. Based on the IR LFs, we then compute the expected number of galaxies with ALMA fluxes larger than the observed source within a redshift interval such that the emission line would lie within 0.2 GHz of the main target's line. As an example, if the emission line of REBELS-29-2 were CO(8-7), the source would lie at $z = 2.73$ and have an infrared luminosity of $\log L_{\rm IR}/L_\odot = 12.0$. Based on the $z \approx 3$ IR LF, one would then expect 3.3×10^{-4} galaxies per random ALMA pointing with a continuum flux larger than what is observed. For all the lines we tested, these numbers turn out to be similarly small ($<6 \times 10^{-4}$ galaxies) for both REBELS-12-2 and REBELS-29-2. Expressed in another way, one would need to observe >1,600 ALMA pointings to find one galaxy with a continuum flux density higher than either of the two serendipitous sources and with an emission line within 0.2 GHz of the primary targets. Hence, we can safely exclude the possibility that these lines stem from random foreground galaxies.

A new parameter space of dusty galaxies

As discussed in the main text, the two sources REBELS-29-2 and REBELS-12-2 are likely to be higher redshift analogues of the dust-obscured galaxies previously identified based on photometric redshifts at $z \approx 3$–6 (ref. [15]). In Extended Data Fig. 3, we compare these sources to different galaxy samples from the literature. In particular, we also show three of the four dusty companion galaxies to $z = 6.0 - 6.6$ quasi-stellar objects (QSOs) reported in Decarli et al.[13] that remained undetected in follow-up rest-frame UV observations[14]. Those sources are likely to be much rarer than our galaxies detected here. The number density of their central QSOs is two orders of magnitude lower than the UV-luminous LBGs of our sample. Additionally, the newly found dusty companions are located at the lower end of QSO companions in terms of infrared and [C II] luminosities. Therefore, as can be seen in Extended Data Fig. 3, our sources at $z \approx 7$ probe a different parameter space in terms of stellar mass and IR luminosities than previous samples.

Even though uncertain, the SEDs of our sources are consistent with being lower luminosity versions of the typical dust-obscured, starburst galaxies at $z \gtrsim 6$ (Fig. 2). Given the current depth of the rest-frame UV images, >97% and >75% of their star formation activities are obscured (95% confidence lower limit). This is in stark contrast to the UV-luminous targets, REBELS-12 and REBELS-29, for which only 39% to 63% of star formation is obscured (see Extended Data Fig. 4). This means that $z \gtrsim 6$ DSFGs need to be searched for in deeper surveys than previously assumed. The main question now is: how common are such lower-luminosity DSFGs in the early Universe? In the next section, we provide several estimates of their contribution to the cosmic SFRD.

Contribution to the cosmic SFR density

The calculation of the cosmic SFRD contributed by the dusty REBELS galaxies is not trivial. In particular, because these galaxies were only

discovered as neighbours to UV-luminous primary sources in our targeted follow-up program. As discussed in the main text, we derive several estimates, which are detailed below.

A somewhat naive, first estimate can be obtained, if we assume that these two sources were detected at random in a blind survey. In this case, the SFRD is simply given by their summed SFR divided by the whole survey volume spanned by the current REBELS dataset. For the survey volume, we integrate over the full frequency ranges over which we scanned for [C II] 158 μm emission lines and we use the area covered by the HPBWs. This totals to a survey volume of 2.3×10^4 Mpc^3. Then, summing the UV+IR-based SFRs of REBELS-29-2 and REBELS-12-2, we obtain $\rho_{SFR} = 5.1 \times 10^{-3}\ M_\odot\ yr^{-1}\ Mpc^{-3}$. Using the [C II]-based SFRs, this amounts to $\rho_{SFR} = 7.8 \times 10^{-3}\ M_\odot\ yr^{-1}\ Mpc^{-3}$. However, as indicated above, these numbers should be taken as upper limits given that REBELS is not a blind survey.

To account for clustering, we can obtain an estimate for the expected boost in number counts (and hence the SFRD) compared to a random, blind survey based on the correlation function[57]. Starting from the real-space correlation function $\xi(r) = (r/r_0)^{-\gamma}$ as measured for $z \approx 7$ galaxies[58], we perform the Limber transform to derive the corresponding angular correlation function[59]. This requires a redshift selection function, which we assume to be a top-hat with redshift depth of $\Delta z = 0.33$, that is., the minimum frequency coverage of the REBELS [C II] line search. The expected number of neighbours in excess of a random field is then derived from this angular correlation function by integrating over a solid angle with radius corresponding to the HPBW (13″). Using the measured correlation function parameters $r_0 = 6.7 \pm 0.9\ h^{-1}$ cMpc and $\gamma = 1.6$, this results in a boost factor due to clustering of $4.1 \pm 0.6\times$. Hence, the SFRD estimates above need to be corrected down by this amount, resulting in $\rho_{SFR} = 1.2 \times 10^{-3}\ M_\odot\ yr^{-1}\ Mpc^{-3}$ or $\rho_{SFR} = 1.9 \times 10^{-3}\ M_\odot\ yr^{-1}\ Mpc^{-3}$, respectively, using the UV+IR based SFRs or the [C II]-derived SFRs.

Unfortunately, the correction factor due to clustering depends quite sensitively on the assumed correlation function parameters, which themselves depend on the mass and luminosity of the sources[60]. For instance, using the simulated correlation function[61] for UV-luminous galaxies with $M_{UV} < -22$ (corresponding to $SFR_{UV} > 24\ M_\odot\ yr^{-1}$), as appropriate for the REBELS primary sample, we derive a boost factor as high as $30\times$. However, we note that these simulations do not include such dusty sources (which have $M_{UV} > -19.4$ and $M_{UV} > -21.4$, respectively), and we will defer the reader to a later paper to estimate an appropriate correlation function for DSFGs such as REBELS-29-2 and REBELS-12-2.

Another, more conservative SFRD estimate of dusty galaxies can be obtained from the fraction of REBELS data cubes that showed such sources, and assuming that these are representative of the cosmic average. Given the existing data from our ongoing program, we currently have [C II] emission lines confirmed in 19 primary targets (at $>6\sigma$). We performed a blind search for other lines in the current dataset, but have only found REBELS-12-2 and REBELS-29-2 without optical counterparts. Hence, for 19 UV-luminous galaxies we found two dust-obscured counterparts with similar masses and SFRs. If we extrapolate this to the full LBG population, this would imply that such dusty sources contribute $10.5^{+9.1}_{-5.0}\%$ of ρ_{SFR}^{MD14}, that is, $8.9^{+7.7}_{-4.3} \times 10^{-4}\ M_\odot\ yr^{-1}\ Mpc^{-3}$. Note that within the large uncertainties, this value is completely consistent with our clustering-corrected SFRDs derived above.

As a final reference, we can also derive an upper limit from the ALMA large program ASPECS, which performed a completely blind line scan over the HUDF, covering [C II] in the redshift range $z = 6 - 8$. This scan would have been sensitive to galaxies with [C II]-based SFRs $\gtrsim 16\ M_\odot\ yr^{-1}$ (5σ detection limit). However, no such sources were found[62]. Using the full ASPECS survey volume, one can thus derive a limit on the total cosmic SFRD from ASPECS down to these SFRs, which results in $<1.0 \times 10^{-2}\ M_\odot\ yr^{-1}\ Mpc^{-3}$.

All the estimates derived above, including the ASPECS blind search, lie significantly below the 'dust-rich' model from Casey et al.[19], which assumes that dust-obscured galaxies contribute ~90% of the total SFR density at $z > 4$. On the other hand, our clustering-corrected estimates are in good agreement with the 'dust-poor' model. However, we note that our sample is limited in SFR and that we needed to extrapolate to lower luminosity sources, as outlined above. At lower redshifts, the fraction of obscured star-formation decreases very rapidly, however, to lower mass and luminosity systems[63,64]. Based on this, it would in principle not be expected that the integration to fainter systems would increase the SFRD of dust-obscured galaxies. However, as we show in Extended Data Fig. 4, the obscured fraction of star-formation may indeed show a much larger variation than previously expected, given that earlier estimates were mostly based on UV-selected samples. Clearly, larger datasets are required to test this further in the future.

Data availability

The datasets generated during and/or analysed during the current study are available from the corresponding author on reasonable request. This paper makes use of the following ALMA data: ADS/JAO. ALMA #2019.1.01634.L.

Code availability

The codes used to reduce and analyse the ALMA data are publicly available. The code used to model the optical-to-infrared SEDs is accessible through GitHub (https://github.com/ACCarnall/bagpipes).

24. McCracken, H. J. et al. UltraVISTA: a new ultra-deep near-infrared survey in COSMOS. *Astron. Astrophys.* **544**, A156 (2012).
25. Jarvis, M. J. et al. The VISTA Deep Extragalactic Observations (VIDEO) survey. *Mon. Not. R. Astron. Soc.* **428**, 1281–1295 (2013).
26. Erben, T. et al. CARS: the CFHTLS-Archive-Research Survey. I. Five-band multi-colour data from 37 sq. deg. CFHTLS-wide observations. *Astron. Astrophys.* **493**, 1197–1222 (2009).
27. Aihara, H. et al. First data release of the Hyper Suprime-Cam Subaru Strategic Program. *Publ. Astron. Soc. Jpn.* **70**, S8 (2018).
28. Bowler, R. A. A. et al. A lack of evolution in the very bright end of the galaxy luminosity function from $z = 8$ to 10. *Mon. Not. R. Astron. Soc.* **493**, 2059–2084 (2020).
29. Stefanon, M. et al. The brightest $z \gtrsim 8$ galaxies over the COSMOS UltraVISTA field. *Astrophys. J.* **883**, 99 (2019).
30. Bowler, R. A. A., Dunlop, J. S., McLure, R. J. & McLeod, D. J. Unveiling the nature of bright $z = 7$ galaxies with the Hubble Space Telescope. *Mon. Not. R. Astron. Soc.* **466**, 3612–3635 (2017).
31. Schaerer, D. et al. The ALPINE-ALMA [C II] survey. Little to no evolution in the [C II]-SFR relation over the last 13 Gyr. *Astron. Astrophys.* **643**, A3 (2020).
32. De Looze, I. et al. The applicability of far-infrared fine-structure lines as star formation rate tracers over wide ranges of metallicities and galaxy types. *Astron. Astrophys.* **568**, A62 (2014).
33. Carnall, A. C., McLure, R. J., Dunlop, J. S. & Davé, R. Inferring the star formation histories of massive quiescent galaxies with BAGPIPES: evidence for multiple quenching mechanisms. *Mon. Not. R. Astron. Soc.* **480**, 4379–4401 (2018).
34. Bruzual, G. & Charlot, S. Stellar population synthesis at the resolution of 2003. *Mon. Not. R. Astron. Soc.* **344**, 1000–1028 (2003).
35. Kroupa, P. & Boily, C. M. On the mass function of star clusters. *Mon. Not. R. Astron. Soc.* **336**, 1188–1194 (2002).
36. Byler, N., Dalcanton, J. J., Conroy, C. & Johnson, B. D. Nebular continuum and line emission in stellar population synthesis models. *Astrophys. J.* **840**, 44 (2017).
37. Ferland, G. J. et al. The 2017 release Cloudy. *Rev. Mexic. Astron. Astrof.* **53**, 385–438 (2017).
38. Calzetti, D. et al. The dust content and opacity of actively star-forming galaxies. *Astrophys. J.* **533**, 682–695 (2000).
39. Charlot, S. & Fall, S. M. A simple model for the absorption of starlight by dust in galaxies. *Astrophys. J.* **539**, 718–731 (2000).
40. Draine, B. T. & Li, A. Infrared emission from interstellar dust. IV. The silicate-graphite-PAH model in the post-Spitzer era. *Astrophys. J.* **657**, 810–837 (2007).
41. Wang, R. et al. Star formation and gas kinematics of quasar host galaxies at $z \sim 6$: new insights from ALMA. *Astrophys. J.* **773**, 44 (2013).
42. Capak, P. L. et al. Galaxies at redshifts 5 to 6 with systematically low dust content and high [C II] emission. *Nature* **522**, 455–458 (2015).
43. Dessauges-Zavadsky, M. et al. The ALPINE-ALMA [C II] survey. Molecular gas budget in the early Universe as traced by [C II]. *Astron. Astrophys.* **643**, A5 (2020).
44. Casey, C. M. Far-infrared spectral energy distribution fitting for galaxies near and far. *Mon. Not. R. Astron. Soc.* **425**, 3094–3103 (2012).
45. Schreiber, C. et al. Dust temperature and mid-to-total infrared color distributions for star-forming galaxies at $0<z<4$. *Astron. Astrophys.* **609**, A30 (2018).
46. Faisst, A. L. et al. ALMA characterises the dust temperature of $z \sim 5.5$ star-forming galaxies. *Mon. Not. R. Astron. Soc.* **498**, 4192–4204 (2020).
47. da Cunha, E. et al. On the effect of the cosmic microwave background in high-redshift (sub-)millimeter observations. *Astrophys. J.* **766**, 13 (2013).

Article

48. Laporte, N. et al. Dust in the reionization era: ALMA observations of a z = 8.38 gravitationally lensed galaxy. *Astrophys. J. Lett.* **837**, L21 (2017).
49. Behrens, C. et al. Dusty galaxies in the epoch of reionization: simulations. *Mon. Not. R. Astron. Soc.* **477**, 552–565 (2018).
50. Liang, L. et al. On the dust temperatures of high-redshift galaxies. *Mon. Not. R. Astron. Soc.* **489**, 1397–1422 (2019).
51. Sommovigo, L. et al. Warm dust in high-z galaxies: origin and implications. *Mon. Not. R. Astron. Soc.* **497**, 956–968 (2020).
52. De Vis, P. et al. A systematic metallicity study of DustPedia galaxies reveals evolution in the dust-to-metal ratios. *Astron. Astrophys.* **623**, A5 (2019).
53. Mancini, M. et al. Interpreting the evolution of galaxy colours from z = 8 to 5. *Mon. Not. R. Astron. Soc.* **462**, 3130–3145 (2016).
54. Graziani, L. et al. The assembly of dusty galaxies at z ≥ 4: statistical properties. *Mon. Not. R. Astron. Soc.* **494**, 1071–1088 (2020).
55. Gruppioni, C. et al. The Herschel PEP/HerMES luminosity function - I. Probing the evolution of PACS selected galaxies to z = 4. *Mon. Not. R. Astron. Soc.* **432**, 23–52 (2013).
56. Carilli, C. L. & Walter, F. Cool gas in high-redshift galaxies. *Annu. Rev. Astron. Astrophys.* **51**, 105–161 (2013).
57. Peebles, P. J. E. *The Large-Scale Structure of the Universe* (Princeton Univ. Press, 1980).
58. Barone-Nugent, R. L. et al. Measurement of galaxy clustering at z ~ 7.2 and the evolution of galaxy bias from 3.8 ~ z ~ 8 in the XDF, GOODS-S, and GOODS-N. *Astrophys. J.* **793**, 17 (2014).
59. Adelberger, K. L. et al. The spatial clustering of star-forming galaxies at redshifts 1.4 < z < 3.5. *Astrophys. J.* **619**, 697–713 (2005).
60. Qiu, Y. et al. Dependence of galaxy clustering on UV luminosity and stellar mass at z ~ 4–7. *Mon. Not. R. Astron. Soc.* **481**, 4885–4894 (2018).
61. Bhowmick, A. K. et al. Cosmic variance of z > 7 galaxies: prediction from BLUETIDES. *Mon. Not. R. Astron. Soc.* **496**, 754–766 (2020).
62. Uzgil, B. D. et al. The ALMA spectroscopic survey in the HUDF: a search for [C II] emitters at 6 ≤ z ≤ 8. *Astrophys. J.* **912**, 67 (2021).
63. Whitaker, K. E. et al. The constant average relationship between dust-obscured star formation and stellar mass from z = 0 to z = 2.5. *Astrophys. J.* **850**, 208 (2017).
64. Fudamoto, Y. et al. The ALPINE-ALMA [CII] survey. Dust attenuation properties and obscured star formation at z ~ 4.4–5.8. *Astron. Astrophys.* **643**, A4 (2020).
65. Béthermin, M. et al. Evolution of the dust emission of massive galaxies up to z = 4 and constraints on their dominant mode of star formation. *Astron. Astrophys.* **573**, A113 (2015).
66. Scoville, N. et al. COSMOS: Hubble Space Telescope observations. *Astrophys. J. Suppl.* **172**, 38–45 (2007).

Extended Data Fig. 1 | Optical/NIR images and full SEDs of the UV-luminous targets REBELS-29 and REBELS-12. The cutouts show images from which photometry was extracted. SED fits (bottom-right panels) are performed using the BAGPIPES[33]. In **b** and **d**, blue solid lines and bands represent the median posterior SEDs together with their 68% confidence contours for REBELS-29 and REBELS-12, respectively. Error bars corresponds to 1σ uncertainties, and downward arrows show 2σ upper limits. **a** and **c** show that the [C II] 158 μm emission line redshifts (red) are in perfect agreement with the photometric redshift probability distributions (blue), that had been previously estimated from the optical/NIR photometry for both sources. This confirms their high-redshift nature.

Article
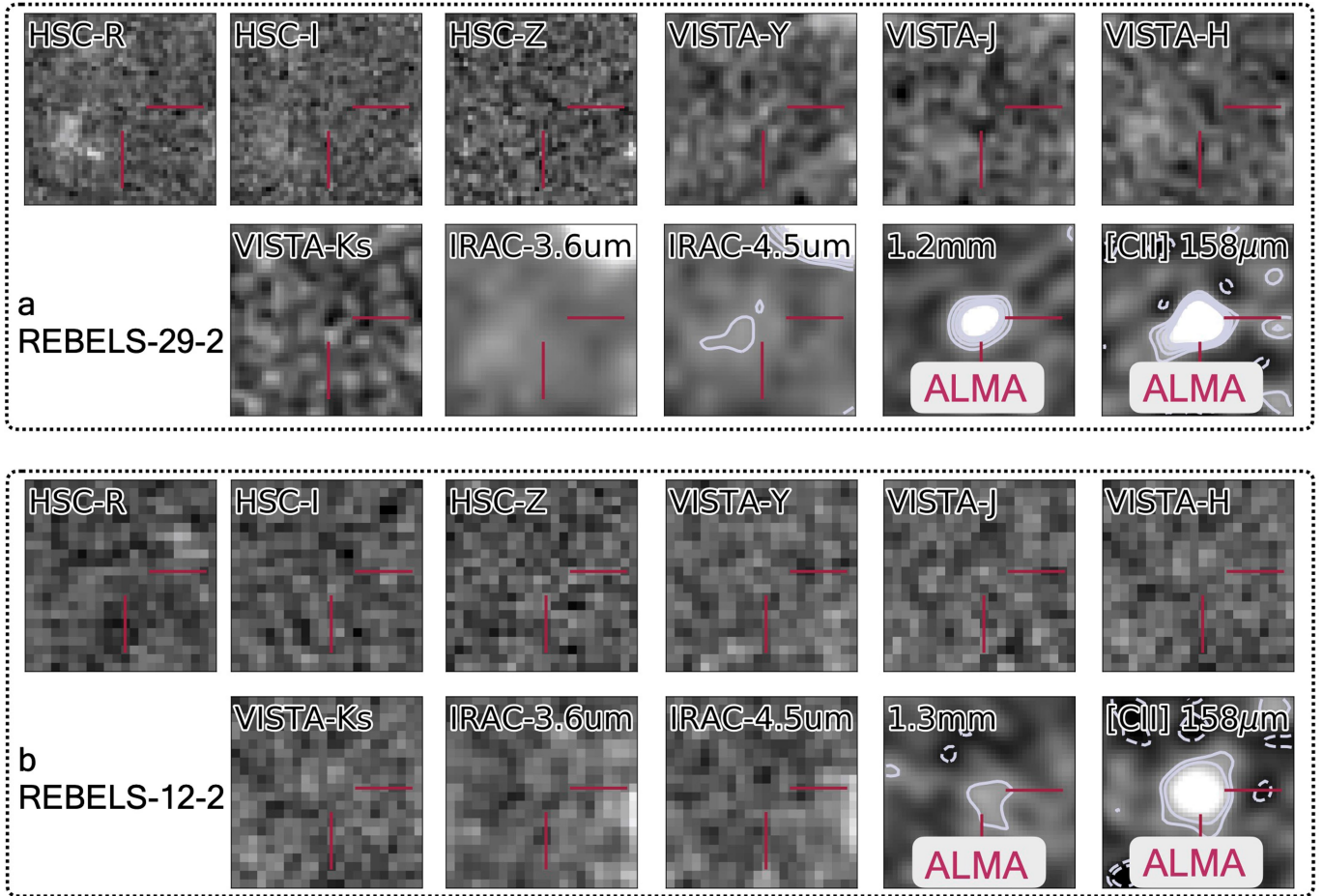
Extended Data Fig. 2 | Optical/NIR/FIR cutouts of the dusty sources REBELS-29-2 and REBELS-12-2. 6.5″ × 6.5″ cutouts show the existing ground- and space-based observations: Subaru Hyper Suprime Cam, VISTA VIRCAM, Spitzer IRAC, in addition to the ALMA dust continuum images and continuum subtracted [C II] 158 μm moment-0 images. White contours show +2, +3, +4, +5 σ (solid contour) and −5, −4, −3, −2 σ (dashed contour), if present. A faint low-surface brightness foreground neighbour can be seen

~2.0″ to the SE of REBELS-29-2. However, the photometric redshift of this foreground source is $z_{ph} = 2.46^{+0.08}_{-0.07}$, and the line frequency of REBELS-29-2 is not consistent with bright FIR emission lines (for example, CO lines) from this foreground redshift. No optical counterparts are found at the location of the ALMA [C II] and dust continuum positions for both REBELS-29-2 and REBELS-12-2.
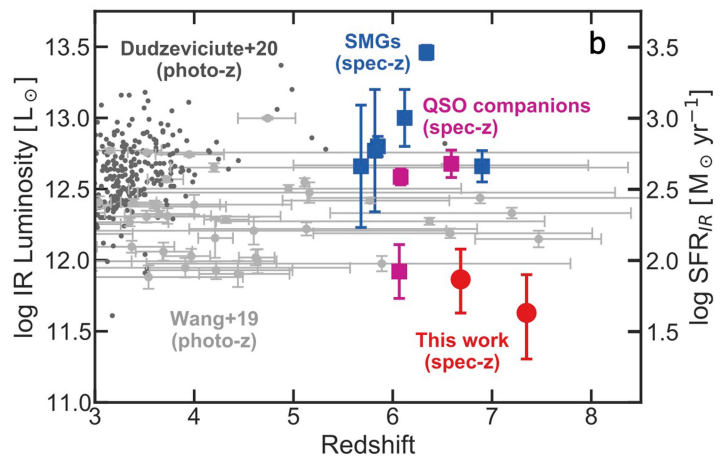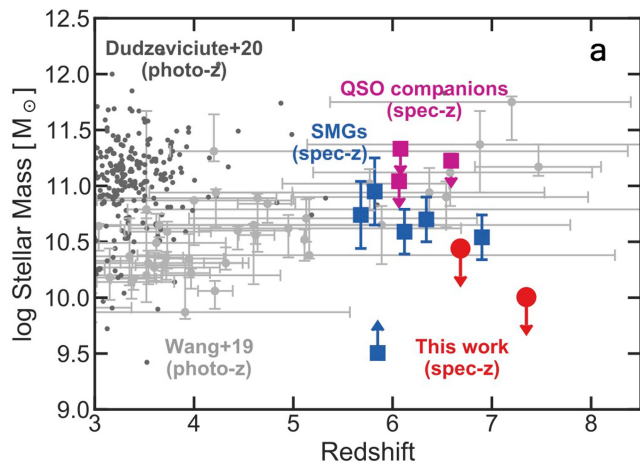
Extended Data Fig. 3 | Probing a new parameter space of DSFGs. a, The stellar mass as a function of redshift for DSFGs from the literature. IRAC-selected, H-dropout galaxies (light-grey dots with 1σ errorbars[15]) are generally more massive than the two serendipitously detected REBELS galaxies (red dots). Additionally, the redshifts of H-dropouts are extremely uncertain (photo-z). The extremely star-bursting SMG population only shows a small tail of rare sources at $z > 4$ (shown by dark dots[11]). The blue squares show all the previously known DSFGs at $z > 5.5$ with spectroscopically measured redshifts, while purple squares correspond to $z \approx 6$ QSO companion galaxies[13]. These are more extreme sources than REBELS-12-2 and REBELS-29-2. **b**, The infrared luminosity/SFR_{IR} as a function of redshift for the same galaxy samples as on the left. The infrared luminosities and hence SFRs of the newly identified galaxies are substantially lower than typical SMGs at these redshifts. For both panels, error bars correspond to 1σ uncertainties, and arrows show 2σ upper/lower limits.
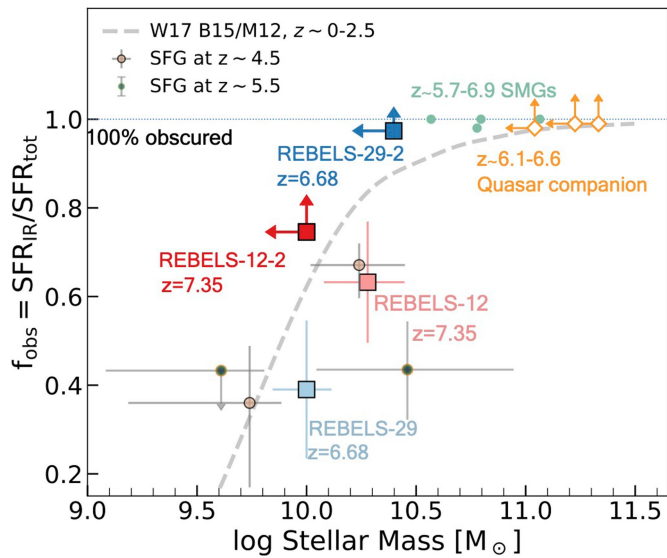
Extended Data Fig. 4 | Fraction of obscured star-formation as a function of stellar mass. The fraction of obscured star-formation, $f_{obs} = SFR_{IR}/(SFR_{IR} + SFR_{UV})$, of REBELS-29-2 and REBELS-12-2 (dark coloured squares) is significantly higher than for typical LBGs at their stellar mass. The line shows the observed, constant relation between $z \approx 0$ and $z \approx 2.5$ (ref. [63]) assuming a given set of SED templates from Bethermin and colleagues[65]. Blue and brown small points with error bars show stacked results of star-forming galaxies at $z \approx 4.5$ and at $z \approx 5.5$, respectively[64]. The star-formation of extreme starburst galaxies at $z \approx 5.7$–6.9 is essentially 100% obscured (SMGs;[12] green small points). The highly obscured star-forming galaxies found as companions of high-redshift quasars at $z > 6$ (refs. [13,14]) (yellow diamonds) are substantially more massive than the galaxies identified here, as estimated from their dynamical masses. Squares show the obscured fraction of our UV-bright and dusty galaxies. Error bars correspond to 1σ uncertainty, and arrows show 2σ lower/upper limits. Our discovery of lower mass, obscured galaxies shows that f_{obs} is likely to vary much more strongly at a fixed stellar mass than previously estimated even in the epoch of reionization.

Extended Data Table 1 | FIR properties observed by ALMA

Galaxy Name	ν_{obs}*	$\sigma_{[CII]}$*	$f_{[CII]}$	f_{cont}	$L_{[CII]}$	L_{IR}	Dust Mass
	(GHz)	(km/s)	(Jy km/s)	(μJy)	(10^8 $L_\odot$)	(10^{11} $L_\odot$)	(10^7 $M_\odot$)
REBELS-29	247.30 ± 0.01	63 ± 9.5	0.44 ± 0.06	61 ± 20	4.86 ± 0.64	$2.21^{+1.85}_{-1.01}$	$0.7^{+0.7}_{-0.4}$
REBELS-29-2	247.39 ± 0.02	142 ± 18	0.78 ± 0.10	192 ± 25	8.56 ± 1.13	$7.33^{+4.63}_{-3.08}$	$2.2^{+2.2}_{-1.1}$
REBELS-12	227.72 ± 0.03	359 ± 45	1.20 ± 0.27	177 ± 52	15.1 ± 3.40	$6.87^{+4.91}_{-2.95}$	$2.1^{+2.3}_{-1.1}$
REBELS-12-2	227.56 ± 0.02	130 ± 21	0.58 ± 0.13	110 ± 52	7.33 ± 1.60	$4.26^{+3.65}_{-2.24}$	$1.2^{+1.7}_{-0.8}$

All values are corrected for the primary beam attenuation and CMB, with T_d=40 K and β=1.5, if necessary.

*ν_{obs} and $\sigma_{[CII]}$ are measured by Gaussian fitting the extracted spectra.

Article

Extended Data Table 2 | NIR photometric data

Band	Wavelength [Å]	REBELS-29*	REBELS-29-2*	REBELS-12[†]	REBELS-12-2[†]	Telescope
g-band	4816.12	0.01 ± 0.02	0.02 ± 0.02	-0.01 ± 0.02	-0.03 ± 0.03	Subaru/HSC
r-band	6234.11	0.01 ± 0.02	0.00 ± 0.02	0.01 ± 0.03	0.00 ± 0.03	Subaru/HSC
i-band	7740.58	0.02 ± 0.03	0.01 ± 0.03	-0.05 ± 0.07	-0.01 ± 0.07	Subaru/HSC
z-band	9125.20	0.00 ± 0.04	-0.04 ± 0.04	0.01 ± 0.19	0.06 ± 0.19	Subaru/HSC
Y-band	10214.19	0.33 ± 0.03	0.05 ± 0.03	0.14 ± 0.08	0.04 ± 0.09	VISTA/VIRCAM
J-band	12534.65	0.41 ± 0.04	-0.03 ± 0.04	0.50 ± 0.11	0.08 ± 0.12	VISTA/VIRCAM
H-band	16453.41	0.34 ± 0.05	-0.08 ± 0.05	0.46 ± 0.15	0.10 ± 0.19	VISTA/VIRCAM
Ks-band	21539.88	0.46 ± 0.06	-0.06 ± 0.06	0.64 ± 0.22	-0.29 ± 0.23	VISTA/VIRCAM
3.6 μm	35634.28	0.70 ± 0.04	0.08 ± 0.05	0.70 ± 0.31	0.13 ± 0.29	Spitzer/IRAC
4.5 μm	45110.13	0.62 ± 0.06	0.14 ± 0.07	1.37 ± 0.41	0.34 ± 0.36	Spitzer/IRAC

Flux densities are shown in units of μJy

*Images are available as a part of the COSMOS survey[66] and UltraVISTA DR4[24]

†Images are available as a part of the VIDEO survey[25].

Extended Data Table 3 | Priors used for panchromatic SED modelling

Assumed Physical Properties	
Initial mass function	Kroupa & Boily
Stellar population synthesis model	Bruzual & Charlot
Dust attenuation law	Calzetti et al.
Star formation history	Constant star formation

Parameters	Priors	Description
Minimum Age	[0.1,1.0]	Time since star formation switched on in Gyr
$\log_{10}$ Stellar Mass	[8.0,12.0]	$\log_{10}$ of stellar mass in solar mass ($M_\odot$)
Metallicity	[0.1,2.5]	in solar metallicity ($Z_\odot$)
A_V	[0.0,10.0]	V band dust attenuation
η	[1.,3]	Multiplicative factor producing extra attenuation for young stars in birth clouds
$\log U$	[-4.0,-2.0]	Starlight intensity on dust grains
U_{min}	[1.0,25.0]	Lower limit of starlight intensity distribution
γ	[0.5,4.0]	Fraction of stars at U_{min}
q_{PAH}	[0.01,0.99]	PAH mass fraction

All priors are uniformly distributed in the range listed in the second column.

The parameters in parentheses are used in independent runs to study the impact of different assumptions.